



Photoelectrochemical properties of BiOCl microplatelets[☆]

Julie Stephenson, Veronica Celorrio, Devendra Tiwari, Simon R. Hall, David C. Green¹, David J. Fermín*

School of Chemistry, University of Bristol, Cantocks Close, Bristol BS8 1TS, UK



A B S T R A C T

The photoelectrochemical properties of highly crystalline and phase-pure BiOCl microplatelets synthesised via a room temperature ionic liquid method are reported. X-ray crystallography reveals a tetragonal BiOCl phase, while high resolution electron microscopy shows sheet-like structures with a cross section of approximately 5 μm and thickness in the range of 500 nm. Diffuse reflectance spectroscopy shows a direct bandgap transition at 3.34 eV. Electrochemical measurements of as-prepared BiOCl powders deposited onto fluorine-doped tin oxide electrodes show a sharp cathodic current at -0.10 V vs RHE at pH 10, which is linked to electron injection into the conduction band edge. Photoelectrochemical measurements in the presence of Na_2SO_3 as hole-acceptor in solution exhibit a strong potential dependence, switching from cathodic to anodic photocurrents at potentials around 0.70 V vs RHE. The positive photocurrent is associated with SO_3^{2-} oxidation, while the unexpected negative photocurrents are linked to cathodic material decomposition.

1. Introduction

The development of stable photoelectrodes for water splitting remains one of the key challenges in material science; an area in which Roger Parsons made valuable contributions in the early 80's [1–4]. Bismuth oxychloride (BiOCl) is a V–VI–VII main group ternary wide-band gap semiconductor oxyhalide composed of Earth abundant materials which has been considered in the context of solar fuels and photocatalysis [5–9]. BiOCl has a tetragonal structure (space group P4/nmm) [6,10,11], comprising slabs of $[\text{Bi}_2\text{O}_2]^{2+}$ interleaved with double layers of chloride ions [12], held together by non-bonding interactions. This structure also gives rise to an internal static electric field, running perpendicular to the layers, which may play a role in the separation of photogenerated charge carriers [13,14]. The conduction band (CB) of BiOCl is dominated by Bi 6p orbitals, while the valence band (VB) is dominated by O 2p and Cl 3p orbitals with additional contribution from Bi orbitals [5,15]. Indeed, one of the interesting properties of Bi oxyhalides, in comparison with other more ionic semiconductor such as TiO_2 , is the hybridised nature of the Bi 6s orbitals dispersed around the top of the VB and the bottom of the CB. This is expected to improve defect tolerance and mobility of photogenerated electron/hole pairs [6].

BiOCl has been primarily investigated in the context of photocatalysis for water remediation [16,17], with reports suggesting higher

stability and activity than the benchmark TiO_2 Degussa P25 catalyst [6,12,18,19]. However, stability in some of the studies is probed by X-ray diffraction, which may not be sensitive enough to changes in surface structure. Other studies have reported changes in the optical properties of the powder under UV illumination, which were linked to the formation of oxygen vacancies [20]. A number of studies have reported enhanced photocatalytic activity in the presence of these so-called oxygen vacancies, although the mechanism underlying these observations remains to be elucidated [21–26]. Ye et al. concluded that the visible absorption induced in BiOCl (“black” BiOCl) is linked to a disordered, reduced outer layer which generates a deep trap state close to the conduction band [22,26]. Several groups have carried out more in-depth studies of surface state defects (both oxygen vacancies and bismuth vacancies) in ultra-thin BiOCl nanosheets and their effect on band gap and recombination [18,27,28].

With regards to BiOCl synthesis, a variety of protocols have been reported based on solvothermal [29,30], hydrothermal [8,31], hydrolysis [6,32], sonochemical [33], electrochemical [13] and vapour deposition methods [34]. These methods generate a variety of particle morphologies and microstructures including nanosheets [35], microdisks [36] and so-called microflowers [8,29]. More recently, a low temperature ionic liquid assisted synthesis has been reported for preparing a variety of bismuth oxyhalide systems [37–39].

In this contribution, we report the photoelectrochemical properties

[☆] In memory of Professor Roger Parsons FRS, FRSC.

* Corresponding author.

E-mail address: David.Fermin@bristol.ac.uk (D.J. Fermín).

¹ Current address: School of Chemistry, University of Leeds, Woodhouse Lane, Leeds LS2 9JT, UK.

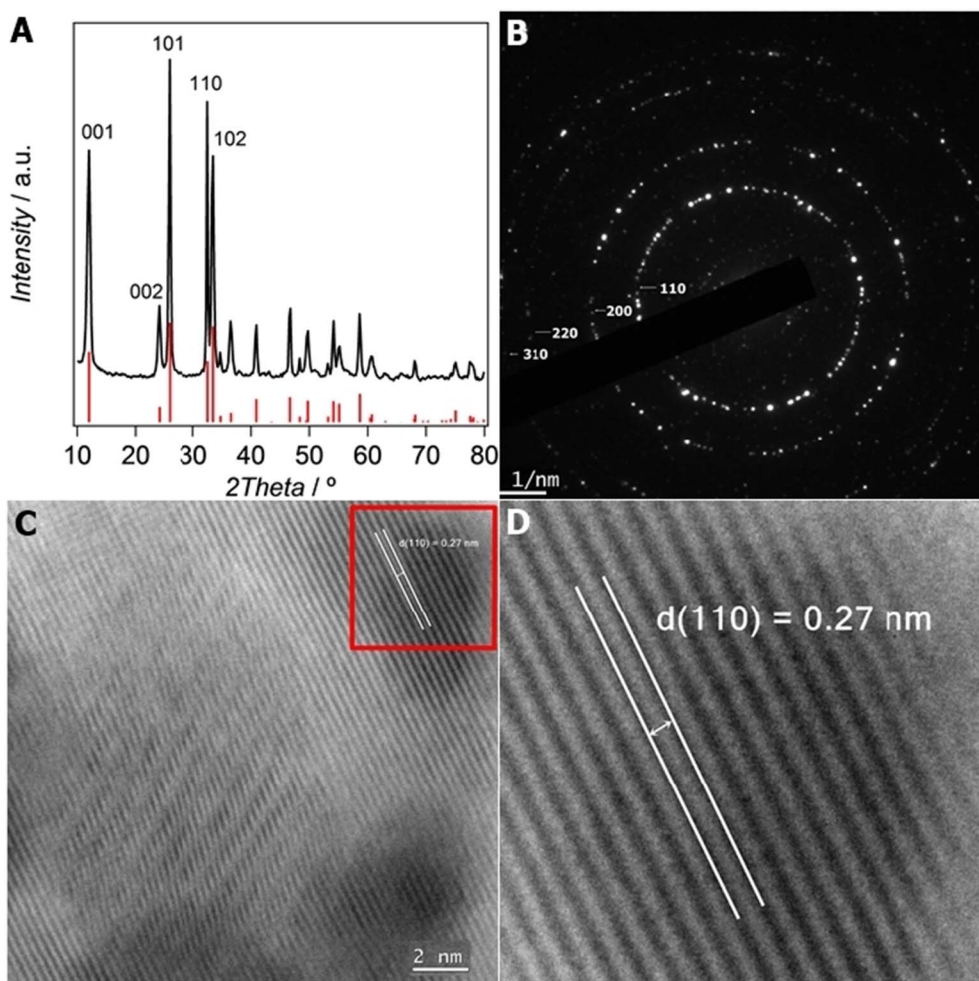


Fig. 1. (A) Powder XRD spectrum for BiOCl showing a match with the standard pattern JCPDS-ICDD File No. 01 085 0861 vertical lines. (B) Electron diffraction pattern of BiOCl showing (110), (200), (220) and (320) planes. (C) HRTEM image displaying lattice fringes and (D) magnification of portion of HRTEM image showing lattice fringes associated with (110) plane (d -spacing 0.27 nm).

of highly phase pure BiOCl microsheets obtained by an ionic liquid based method requiring low temperatures, ambient pressure and a short synthesis time. The as-grown material exhibits fascinating microstructure features such as Moiré fringes in transmission electron microscopy arising from stacking of the platelet structure. Thin films obtained by spin-coating and low temperature sintering onto F-doped SnO₂ electrodes (FTO) were characterised by cathodic currents at potentials more negative than 0.05 V vs RHE, which is associated with electron injection into the conduction band of BiOCl. Electrochemical features emerging from electron injection into the conduction band provide evidence of cathodic surface decomposition, leading to the formation Bi sites. Photoelectrochemical responses were investigated in the presence of Na₂SO₃, a strong hole-acceptor which can minimise photoanodic decomposition of the material and surface recombination losses [40]. Unexpectedly, transient photocurrent under UV illumination were characterised by a sharp potential dependence featuring anodic and cathodic photoresponses. We rationalised the complex potential dependence of the photocurrent in terms of carrier transport and photoelectrochemical stability of the material.

2. Experimental

BiOCl microplatelets were synthesised via a low temperature method using 1-butyl, 3-methylimidazolium chloride as solvent [41–45]. Ionic liquid based synthesis is extremely versatile, enabling to dissolve a variety of metal precursors including highly acidic Bi salts in anhydrous conditions. 1-Butyl, 3-methylimidazolium chloride was prepared by mixing 1-methylimidazole (9.96 ml, 0.125 mol) ($\geq 99\%$,

Sigma Aldrich) with 1-chlorobutane (22.93 ml, 0.15 mol) (anhydrous, 99.5%, Sigma Aldrich) in acetonitrile (20 ml) and refluxed (70 °C) for 24 h, with constant stirring. The solvent was then removed by rotary evaporation at 45 °C. The remaining liquid was washed with a large excess of cold ethyl acetate, and centrifuged at 8000 rpm for 2 min. The ionic liquid is collected from the lower layer. To prepare BiOCl, 1 ml of 1-butyl, 3-methylimidazolium chloride was heated under stirring at 80 °C to achieve dehydration. After 1 h, 105 mg Bi(NO₃)₃·5H₂O (reagent grade, 98%, Sigma Aldrich) was added and stirred at 80 °C until completely dissolved, yielding a clear solution without precipitants. Water was then added dropwise to the solution under stirring and white powder precipitated. The white BiOCl powder was collected by centrifugation and washed several times with ethanol.

X-ray diffraction (XRD) patterns were recorded using a Bruker AXS D8 Advance diffractometer with a θ - θ configuration and using CuK α radiation ($\lambda = 0.154$ nm). Transmission electron microscopy (TEM) studies were carried out using a JEOL JEM-1400Plus microscope and high resolution TEM (HRTEM) studies were performed with a JEOL JEM. Samples for TEM were prepared by placing 1 μ l drops of the BiOCl particles dispersed in a 1:1 mix of ethanol and water on a 3 mm diameter carbon-coated copper grid. UV/Vis diffuse reflectance spectra were recorded using a Shimadzu UV-2600 UV-Vis Spectrophotometer.

Thin films in the range 2–3 μ m were prepared by spin-coating 150 μ l BiOCl suspension (150 mg suspended in 2 ml terpineol) onto a clean 1 cm² area of fluorine doped tin oxide (FTO). A Pt wire was used as a counter electrode and an Ag/AgCl placed in a lugging capillary as a reference electrode. Photocurrent measurements were conducted in Ar-saturated Na₂SO₃ aqueous solutions at pH 10, using an Ivium

CompactStat. All potentials have been converted to RHE. A single compartment glass cell fitted with a quartz window was used in the photoelectrochemical studies. Illumination was provided using a LED with a narrow emission centred at 311 nm (Thorlabs) or a Newport 150 Watt Xenon Arc lamp in conjunction with a constant power supply (Bentham 605) and a monochromator (Bentham TMc300) and optical chopper (Scitec Instruments).

3. Results and discussion

Fig. 1A shows the powder XRD pattern of as-prepared BiOCl, featuring a strong correlation with the tetragonal phase JCPDS-ICDD File No. 01-085-0861. No other peaks are observed linked to the presence of secondary phases. Fig. 1B displays the electron diffraction pattern from which it is possible to determine the (110), (200), (220) and (120) planes with d -spacings of 0.275 nm, 0.193 nm, 0.137 nm and 0.121 nm respectively. The TEM image in Fig. 1C exhibits lattice fringes associated with the (110) plane which are further magnified in Fig. 1D. The fact that the (110) plane is the most prominent feature in the TEM images is consistent with the strong XRD peaks in Fig. 1A. The d -spacing for the (110) plane obtained from XRD, electron diffraction and TEM are fully consistent.

The SEM image in Fig. 2A reveals the flake-like morphology of the as-prepared BiOCl powder. The TEM micrograph in Fig. 2B shows BiOCl sheets with diameter of 540 ± 160 nm. Fig. 2B shows most of the particles lying flat, with a small number of particles appearing as spikes when seen edge-on. The inset in Fig. 2B highlights an edge-on particle with a thickness of 20.8 ± 0.87 nm. Moiré fringes can clearly be seen

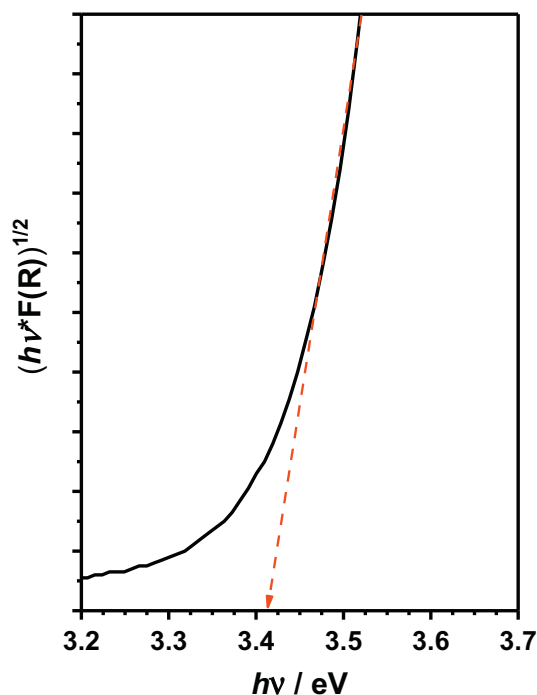


Fig. 3. Tauc plot for BiOCl obtained from diffuse reflectance employing the Kubelka-Munk function ($F(R)$). A bandgap of 3.41 eV was estimated from the intercept in the x-axis.

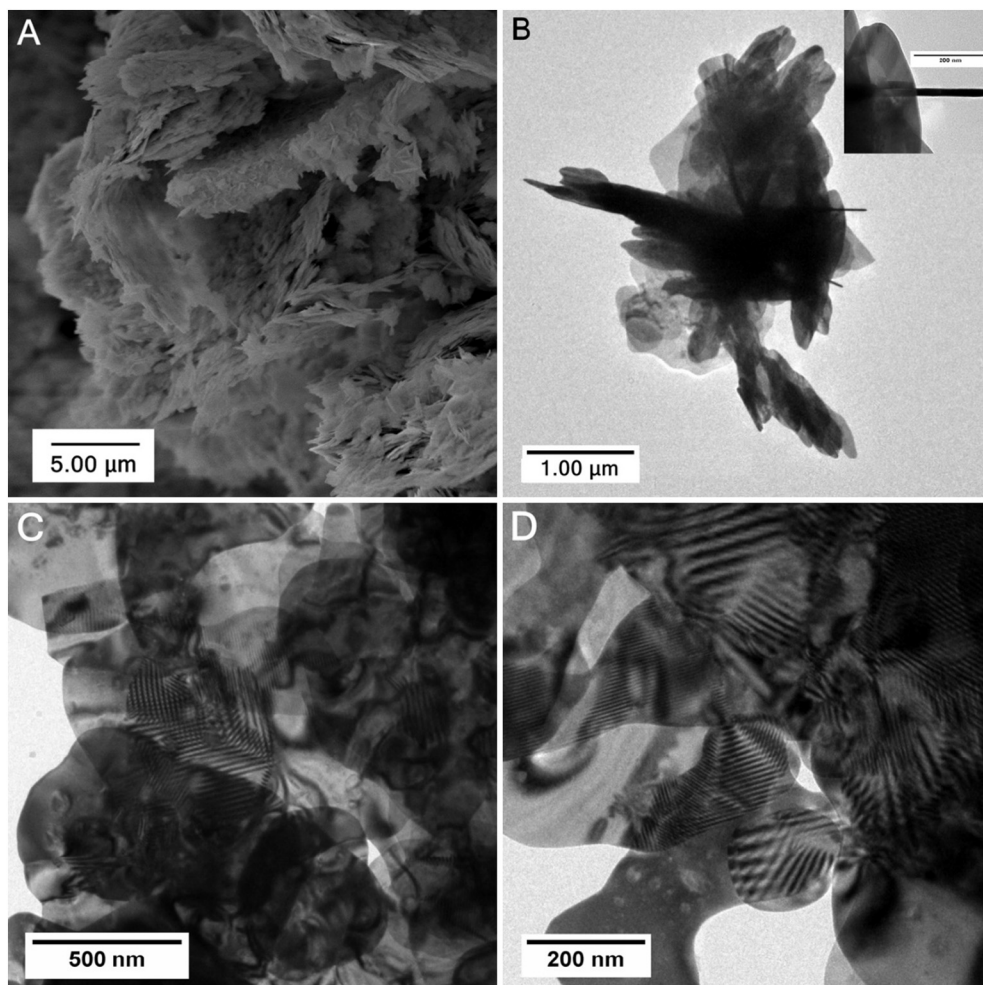


Fig. 2. (A) SEM image showing the BiOCl sheets comprising smaller flakes. (B) TEM images showing BiOCl sheets, flat and side on. (C) and (D) Moiré fringes caused by rotation between overlapping crystals.

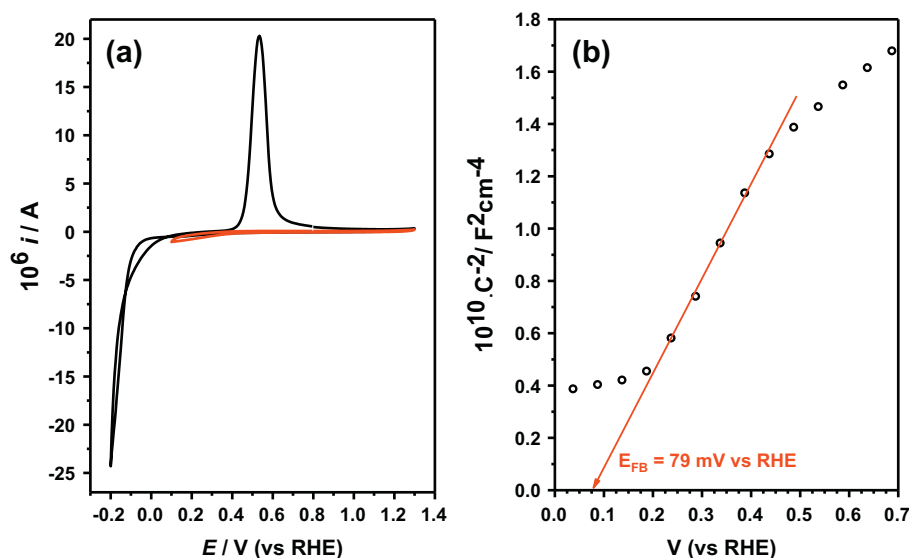


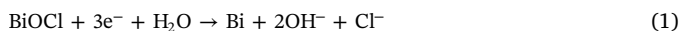
Fig. 4. Cyclic voltammograms (a) and Mott-Schottky plot (b) of BiOCl deposited onto FTO carried out in Ar-saturated 0.1 M Na₂SO₄ at pH 10 in the absence of light. Cyclic voltammograms were recorded with two different electrodes, setting the initial potential close to 0.9 V and scanning to 0.1 (red trace) and -0.2 V (black trace) at 50 mV s^{-1} . The capacitance data used for the Mott-Schottky plots were extracted from impedance responses over a range of 67 Hz to 3768 Hz. (For interpretation of the references to colour in this figure legend, the reader is referred to the web version of this article.)

in Fig. 2C and Fig. 2D with a characteristic spacing of $7.9 \pm 1.5 \text{ nm}$. These fringes are caused either by rotation between overlapping crystals or, in an open structure such as BiOCl, by rotation between the layers of the crystal.

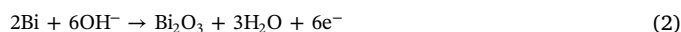
Fig. 3 shows a Tauc plot [46] constructed from diffuse reflectance measurements. The analysis shows a linear relationship of the Kubelka-Munk function with the excitation energy, consistent with an indirect transition at the band gap energy. The estimated band gap value was 3.41 eV ($\sim 364 \text{ nm}$) in agreement with the value calculated using hybrid functional including relativistic treatment [15].

Fig. 4a shows a cyclic voltammograms of BiOCl in a 0.1 M Na₂SO₄ solution at pH 10 in the absence of light. The initial potential was set at 0.81 V vs RHE, scanning in the negative direction at a rate of 50 mV s^{-1} . Upon scanning to potential more negative than -0.10 V , a sharp cathodic response can be observed. In the reverse scan (positive direction), the voltammogram features a well-defined anodic peak centred at 0.47 V. The anodic feature is only observed upon scanning the potential more negative than -0.10 V . The red trace, obtained with a fresh sample, shows that if the potential is reversed at 0.10 V, then no anodic response is detected on the reverse scan. This behaviour clearly shows that changes in the composition at the semiconductor surface occur upon electron injection at potentials below 0.10 V. Cathodic corrosion of semiconductor electrodes has also been reported on a variety of materials such as II–VI quantum dots [47] further demonstrating that systematic analysis of voltammetric responses is essential to distinguish intrinsic electronic states from those generated by electrochemical reactions.

Mott-Schottky plot constructed from analysis of impedance data in the frequency range of 67 to 3786 Hz is shown in Fig. 4b. The plot exhibit with positive slope consistent with a n-type semiconducting behaviour. The flat band potential is located at 79 mV vs RHE (4.52 eV vs Vacuum) which is close to the onset of the cathodic current in the cyclic voltammogram (Fig. 4a). This value is also consistent with the electron affinity of 4.5 eV calculated for BiOCl, which is also in the range typically observed for a variety of n-type semiconductors [15]. This behaviour confirms that the sharp cathodic current at -0.10 V vs RHE can be associated with electron accumulation into the conduction band of BiOCl. The conduction band is dominated by Bi (III) orbitals, leading to the generation of metallic Bi at the surface,



The standard potential for Reaction (1) is 0.16 V vs RHE. In the reverse reaction, Bi sites are oxidised to Bi(III) giving rise to the peak current centred at 0.47 V,



This observation is in accordance with the Pourbaix diagram for Bi [48]. Considering an optical band gap of 3.34 eV and setting the conduction band edge at 79 mV vs RHE, the valance band edge is expected to be at 3.42 V. Recent reports have claimed p-type behaviour of BiOCl based on Mott-Schottky plots [49,50], with flat band potential values above 2 V vs RHE. Such unrealistic flat band potential values for a p-type semiconductor is a clear indication that the capacitance measurements are affected by Fermi level pinning most probably connected to high density of Bi sites.

Fig. 5 displays a linear potential scan at 1 mV s^{-1} in the negative direction in Ar-saturated 0.1 M Na₂SO₃ solution at pH 10 under square-wave illumination. The BiOCl film was illuminated through the electrolyte solution with a LED featuring a narrow wavelength emission centred at 311 nm and a photon flux of $9.56 \times 10^{14} \text{ cm}^{-2} \text{ s}^{-1}$. Photocurrent responses are observed across the full potential range. Intriguingly, the photocurrent switches from anodic to cathodic values at potentials close to 0.7 V vs RHE. This behaviour has not been reported previously, which is even more surprising given the high concentration of SO_3^{2-} . As mentioned above, SO_3^{2-} is a swift hole acceptor that

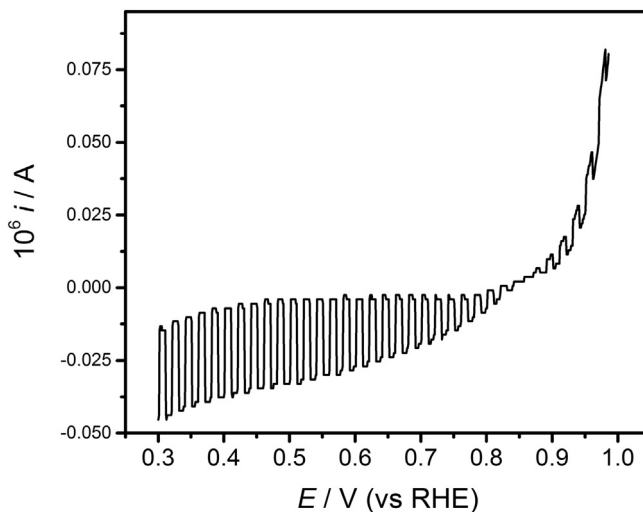


Fig. 5. Linear sweep potential of BiOCl electrode under light perturbation carried out in the cathodic direction. Measurement recorded at 1 mV s^{-1} in an Ar-saturated 0.1 M Na₂SO₃ solution at pH 10. Illumination using a square wave with frequency, photon flux and wavelength of 0.05 Hz, $3.8 \times 10^{13} \text{ cm}^{-2} \text{ s}^{-1}$ and 311 nm respectively.

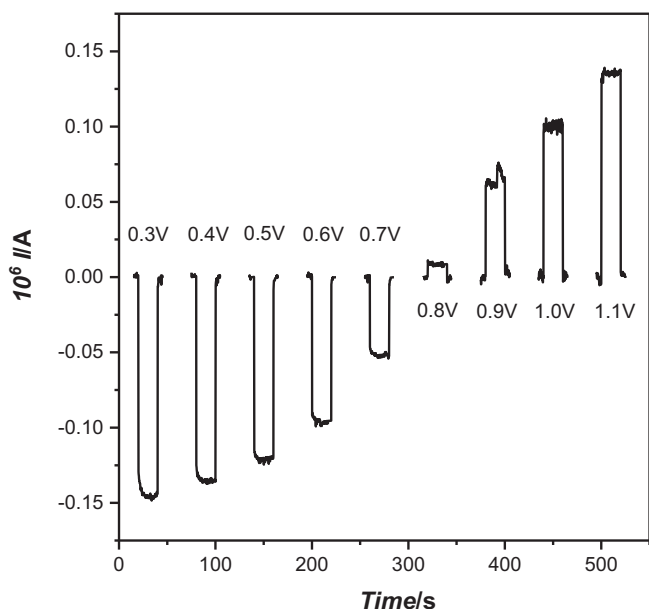


Fig. 6. Transient photocurrent responses at different applied potentials and a photon flux of $3.8 \times 10^{13} \text{ cm}^{-2} \text{ s}^{-1}$.

promotes stabilisation of n-type semiconductors under illumination [40]. In the case of SO_4^{2-} (i.e. water oxidation), the anodic photocurrents are somewhat dampened although further experiments are required to establish a more quantitative analysis of the difference in hole-extraction rate.

In order to ensure that the origin of the photocurrent reversal was not linked to rather high bias, photocurrent transients were recorded with a fresh film in the potential range close to 0.8 V. As shown in Fig. 6, the behaviour is clearly reproduced with a sharp transition between 0.7 and 0.8 V. The same photocurrent reversal is observed under oxygen saturated solutions, indicating that the cathodic photocurrents are associated with the BiOCl reduction (triggering Reaction (2)), rather than oxygen reduction. It is also observed that applying a more negative potential under illumination causes a change in the BiOCl film, from a pearlescent white appearance to silver/grey, confirming that BiOCl is being reduced.

The photocurrent spectra of BiOCl in a 0.1 M Na_2SO_3 solution at 0.4, 0.6, 0.8 V (vs RHE) are contrasted in Fig. 7. It can be seen that the photocurrent onset is located around 370 nm, which is consistent with the optical bandgap (3.34 eV). Consequently, both photoanodic and photocathodic responses originate from the generation of charge carriers under band-gap illumination. It is also observed that the photocathodic responses have a larger magnitude and sharper potential dependence as shown in Figs. 5 and 6. The cathodic photocurrent is thus attributed to a photocathodic corrosion of the electrode, where some of the Bi^{3+} is being reduced to Bi metal (Reaction (2)), whereas the anodic photocurrent is attributed to SO_3^{2-} oxidation.

As discussed previously, reduced Bi sites can be generated upon injecting electrons into the conduction band of BiOCl. At potentials above 1 V, the surface states associated Bi_2O_3 states are effectively empty, opening a pathway to electron from SO_3^{2-} to be injected under illumination. In other words, hole transfer to SO_3^{2-} is facilitated by the surfaces Bi_2O_3 states. As the potential is shifted to more negative values, the Bi_2O_3 states are populated, decreasing the probability of hole transfer to SO_3^{2-} . Under these conditions, the probability of photo-generated electrons to reduce BiOCl sharply increases, leading to photocathodic responses. The Bi_2O_3 mediated hole transfer mechanism is most probably linked to the fact that the valence band orbitals of BiOCl lie very deep in energy with very little overlap with the sulphite orbitals.

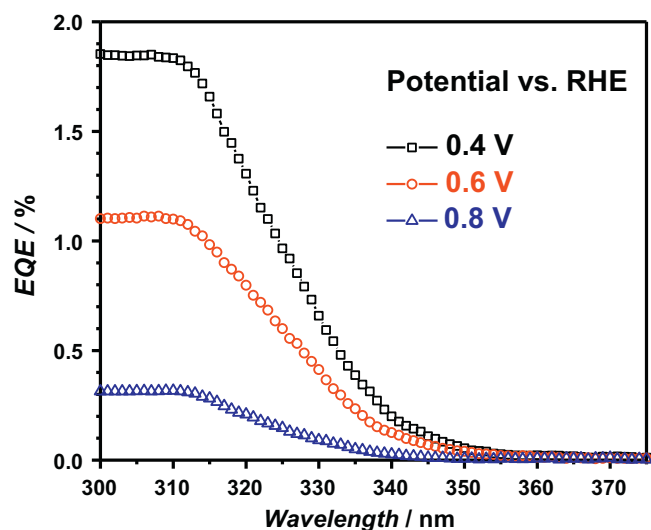


Fig. 7. External quantum efficiency as a function of illumination wavelength for BiOCl films at different applied potentials between 0.4, 0.6, 0.8 V vs RHE, in an Ar-saturated 0.1 M Na_2SO_3 solution at pH 10.

Finally, the maximum quantum yield for the photoanodic and photocathodic responses were 0.3% and 1.8%, at wavelength below 310 nm. These values suggest significant recombination losses, most probably in the bulk of the film. Integrating the EQE spectra recorded at 0.4 V, we could estimate photocurrent responses in the range of $10.5 \mu\text{A cm}^{-2}$ under AM 1.5G illumination. It is rather complex to benchmark this value with respect to reports in the literature given the significant differences in the experimental conditions and morphology of the electrodes. A recent study by Bachu et al. also mentioned the switch of photocathodic to photoanodic responses, reporting a value of $100 \mu\text{A cm}^{-2}$ at approximately 1.8 V vs RHE under 100 mW cm^{-2} illumination [49]. The data reported by Fan and co-workers are difficult to rationalize given that the BiOCl film was connected to the counter-electrode in a three-electrode potentiostatic assembly [50]. Liu et al. obtained photocurrent values below $0.5 \mu\text{A cm}^{-2}$ for BiOCl heterostructure featuring two different phases, however the potential and illumination levels are not specified in the report [51].

Based on these observations, we conclude that pristine BiOCl particles are unsuitable as photoelectrodes for the water-splitting reaction, mainly due to the low-lying conduction band edge and the pore charge transport in highly textured films. However, metallic Bi sites are spontaneously generated under illumination in aqueous solutions which can potentially catalyse the hydrogen evolution or oxygen reduction reaction. It could be envisaged that under appropriate illumination levels and electrolyte composition, stable photocatalytic performance can be achieved by these materials. An alternative strategy to improve performance is to facilitate transport of majority carriers by generating composite materials, e.g. high surface area carbon [52,53].

4. Conclusions

This study reports on the photoelectrochemical responses of BiOCl thin films prepared by an ionic liquid synthesis method. This room temperature method generates crystalline, tetragonal phase BiOCl micro-platelets with the (110) plane being the most prominent. Thin-films were prepared by spin-coating onto F:SnO₂ electrodes, showing a cathodic response at -0.1 V vs RHE assigned to electron injection into the conduction band edge. Potential dependence of the capacitance also suggests that the flat band potential is located at 0.079 V. Interestingly, electron injection into the conduction band leads to the appearance of a broad anodic peak at 0.47 V, which is linked to the oxidation of surface Bi sites. This peak suggests that electron accumulation leads to the

cathodic decomposition of BiOCl, yielding metallic Bi sites.

Photoelectrochemical responses in the presence of Na₂SO₃ at pH 10 show a complex potential dependence across the range between 0.30 V and 1.10 V. At potentials above 0.7 V, the photocurrent is anodic and linked to the oxidation of SO₃²⁻. As the potential is shifted more negative, the photocurrent sign sharply switches to negative values. Comparing the potential dependence of photocurrent with the cyclic voltammogram in the dark, the reversal of the photocurrent sign occurs at the onset of reduction of Bi oxide surface sites. This interesting observation suggest that hole-injection to SO₃²⁻ is mediated by surface Bi-oxide sites. Once electrons are populated in these sites, i.e. at potentials more negative than 0.7 V, the generation of metallic Bi promotes negative photocurrent responses. This photocathodic signals are most probably connected to further decomposition of BiOCl to form metallic Bi.

Acknowledgements

The authors are grateful to the support by Dr. Kieren Bradley and Dr. David Parker during the early stages of this work, and to Mr. Jonathan A. Jones for his contribution of the electron microscopy studies. J.S. thanks the School of Chemistry for awarding a PhD Studentship funded by the Engineering and Physical Science Research Council (Grant number 1247175). V.C. gratefully acknowledges the Royal Society and the UK National Academy for the support through the Newton Fellowship program (NF120002). D.T. and D.J.F. are indebted to EPSRC for financial support through the PVTEAM programme (EP/L017792). V.C. and D.J.F. also acknowledge the EPSRC support via the UK Catalysis Hub (EP/K014706/1 and EP014714/1). Electron microscopy studies were performed with equipment funded by EPSRC through the grant “Atoms to Applications” (EP/K035746/1).

References

- H. Ezzouia, R. Heindl, R. Parsons, H. Tributsch, Studies on the stability of RuS₂ single crystals and the photo-oxidation of halides, *J. Electroanal. Chem.* 165 (1984) 155–166.
- B. Fotouhi, A. Katty, R. Parsons, Current—voltage and capacitance—voltage characteristics of n-SnS₂ single crystals in aqueous solutions containing different redox reagents, *J. Electroanal. Chem.* 183 (1985) 303–314.
- M. Etman, C. Koehler, R. Parsons, A pulse method for the study of the semiconductor-electrolyte interface, *J. Electroanal. Chem.* 130 (1981) 57–66.
- R. Guittard, R. Heindl, R. Parsons, M.A.M. Redon, H. Tributsch, Ruthenium disulphide as a photoelectrode, *J. Electroanal. Chem.* 111 (1980) 401–403.
- S.Y. Chai, Y.J. Kim, M.H. Jung, A.K. Chakraborty, D. Jung, W.I. Lee, Heterojunctioned BiOCl/Bi₂O₃, a new visible light photocatalyst, *J. Catal.* 262 (2009) 144–149.
- K.-L. Zhang, C.-M. Liu, F.-Q. Huang, C. Zheng, W.-D. Wang, Study of the electronic structure and photocatalytic activity of the BiOCl photocatalyst, *Appl. Catal. B Environ.* 68 (2006) 125–129.
- S.K. Poznyak, A.I. Kulak, Photoelectrochemical properties of bismuth oxyhalide films, *Electrochim. Acta* 35 (1990) 1941–1947.
- D.-H. Wang, G.-Q. Gao, Y.-W. Zhang, L.-S. Zhou, A.-W. Xu, W. Chen, Nanosheet-constructed porous BiOCl with dominant {001} facets for superior photosensitized degradation, *Nano* 4 (2012) 7780–7785.
- L. Ye, H. Wang, X. Jin, Y. Su, D. Wang, H. Xie, X. Liu, X. Liu, Synthesis of olive-green few-layered BiOI for efficient photoreduction of CO₂ into solar fuels under visible/near-infrared light, *Sol. Energy Mater. Sol. Cells* 144 (2016) 732–739.
- X. Zhang, L. Zhao, C. Fan, Z. Liang, P. Han, Effects of oxygen vacancy on the electronic structure and absorption spectra of bismuth oxychloride, *Comput. Mater. Sci.* 61 (2012) 180–184.
- X. Zhang, L. Zhao, C. Fan, Z. Liang, P. Han, First-principles investigation of impurity concentration influence on bonding behavior, electronic structure and visible light absorption for Mn-doped BiOCl photocatalyst, *Physica B* 407 (2012) 4416–4424.
- X. Zhang, Z. Ai, F. Jia, L. Zhang, Generalized one-pot synthesis, characterization, and photocatalytic activity of hierarchical BiOX (X = Cl, Br, I) nanoplate microspheres, *J. Phys. Chem. C* 112 (2008) 747–753.
- X. Zhang, X. Liu, C. Fan, Y. Wang, Z. Liang, A novel BiOCl thin film prepared by electrochemical method and its application in photocatalysis, *Appl. Catal. B Environ.* 132 (2013) 332–341.
- M. Li, J. Zhang, H. Gao, F. Li, S.-E. Lindquist, N. Wu, R. Wang, Microsized BiOCl Square Nanosheets as ultraviolet photodetectors and photocatalysts, *ACS Appl. Mater. Interfaces* 8 (2016) 6662–6668.
- A.M. Ganose, M. Cuff, K.T. Butler, A. Walsh, D.O. Scanlon, Interplay of orbital and relativistic effects in bismuth oxyhalides: BiOF, BiOCl, BiOBr, and BiOI, *Chem. Mater.* 28 (2016) 1980–1984.
- Z. Xu, W. Hao, Q. Zhang, Z. Fu, H. Feng, Y. Du, S. Dou, Indirect-direct band transformation of few-layer BiOCl under biaxial strain, *J. Phys. Chem. C* 120 (2016) 8589–8594.
- T. Jing, Y. Dai, X. Ma, W. Wei, B. Huang, The photocatalytic properties of ultrathin bismuth oxychloride nanosheets: a first principles study, *Phys. Chem. Chem. Phys.* 18 (2016) 7261–7268.
- M. Guan, C. Xiao, J. Zhang, S. Fan, R. An, Q. Cheng, J. Xie, M. Zhou, B. Ye, Y. Xie, Vacancy associates promoting solar-driven photocatalytic activity of ultrathin bismuth oxychloride nanosheets, *J. Am. Chem. Soc.* 135 (2013) 10411–10417.
- J. Jiang, K. Zhao, X. Xiao, L. Zhang, Synthesis and facet-dependent photoreactivity of BiOCl single-crystalline nanosheets, *J. Am. Chem. Soc.* 134 (2012) 4473–4476.
- L. Ye, L. Zan, L. Tian, T. Peng, J. Zhang, The {001} facets-dependent high photoreactivity of BiOCl nanosheets, *Chem. Commun.* 47 (2011) 6951–6953.
- L. Chen, S.-F. Yin, R. Huang, Y. Zhou, S.-L. Luo, C.-T. Au, Facile synthesis of BiOCl nano-flowers of narrow band gap and their visible-light-induced photocatalytic property, *Catal. Commun.* 23 (2012) 54–57.
- L. Ye, K. Deng, F. Xu, L. Tian, T. Peng, L. Zan, Increasing visible-light absorption for photocatalysis with black BiOCl, *Phys. Chem. Chem. Phys.* 14 (2012) 82–85.
- H. An, Y. Du, T. Wang, C. Wang, W. Hao, J. Zhang, Photocatalytic properties of BiOX (X = Cl, Br, and I), *Rare Metals* 27 (2008) 243–250.
- M. Zimbone, G. Cacciato, R. Sanz, R. Carles, A. Gulino, V. Privitera, M.G. Grimaldi, Black TiO₂ photocatalyst obtained by laser irradiation in water, *Catal. Commun.* 84 (2016) 11–15.
- Y. Li, C. Li, Z. Zhang, Y. Zhang, X. Sun, H. Si, J. Zhang, Black BiOCl with disorder surface structure prepared by Fe reduction and the enhanced photocatalytic activity, *Solid State Sci.* 34 (2014) 107–112.
- L. Ye, X. Jin, Y. Leng, Y. Su, H. Xie, C. Liu, Synthesis of black ultrathin BiOCl nanosheets for efficient photocatalytic H₂ production under visible light irradiation, *J. Power Sources* 293 (2015) 409–415.
- L. Zhang, Z. Han, W. Wang, X. Li, Y. Su, D. Jiang, X. Lei, S. Sun, Solar-light-driven pure water splitting with ultrathin BiOCl nanosheets, *Chem. Eur. J.* 21 (2015) 18089–18094.
- J. Xu, Y. Teng, F. Teng, Effect of Surface Defect States on Valence Band and Charge Separation and Transfer Efficiency, Vol. 6 (2016), p. 32457.
- L.-P. Zhu, G.-H. Liao, N.-C. Bing, L.-L. Wang, Y. Yang, H.-Y. Xie, Self-assembled 3D BiOCl hierarchical structures: tunable synthesis and characterization, *CrystEngComm* 12 (2010) 3791–3796.
- Q. Mu, Q. Zhang, H. Wang, Y. Li, Facile growth of vertically aligned BiOCl nanosheet arrays on conductive glass substrate with high photocatalytic properties, *J. Mater. Chem.* 22 (2012) 16851–16857.
- X. Xiao, C. Liu, R. Hu, X. Zuo, J. Nan, L. Li, L. Wang, Oxygen-rich bismuth oxyhalides: generalized one-pot synthesis, band structures and visible-light photocatalytic properties, *J. Mater. Chem.* 22 (2012) 22840–22843.
- X. Liu, C. Fan, Y. Wang, Y. Wang, X. Zhang, Z. Liang, Low temperature preparation of flower-like BiOCl film and its photocatalytic activity, *SCIENCE CHINA Chem.* 55 (2012) 2438–2444.
- J. Geng, W.-H. Hou, Y.-N. Lv, J.-J. Zhu, H.-Y. Chen, One-dimensional BiPO₄ nanorods and two-dimensional BiOCl lamellae: fast low-temperature sonochemical synthesis, characterization, and growth mechanism, *Inorg. Chem.* 44 (2005) 8503–8509.
- C. Sihai, G. Chuanfei, L. Ying, G. Yanjun, L. Qian, A novel BiOCl film with flowerlike hierarchical structures and its optical properties, *Nanotechnology* 20 (2009) 275702.
- J. Ma, X. Liu, J. Lian, X. Duan, W. Zheng, Ionothermal synthesis of BiOCl nanostructures via a long-chain ionic liquid precursor route, *Cryst. Growth Des.* 10 (2010) 2522–2527.
- S. Peng, L. Li, P. Zhu, Y. Wu, M. Srinivasan, S.G. Mhaisalkar, S. Ramakrishna, Q. Yan, Controlled synthesis of BiOCl hierarchical self-assemblies with highly efficient photocatalytic properties, *Chem. Asian J.* 8 (2013) 258–268.
- X. Yu, J. Yang, K. Ye, X. Fu, Y. Zhu, Y. Zhang, Facile one-step synthesis of BiOCl/BiOI heterojunctions with exposed {001} facet for highly enhanced visible light photocatalytic performances, *Inorg. Chem. Commun.* 71 (2016) 45–49.
- C. Yang, F. Li, T. Li, W. Cao, Ionic-liquid assisted ultrasonic synthesis of BiOCl with controllable morphology and enhanced visible light and sunlight photocatalytic activity, *J. Mol. Catal. A Chem.* 418 (2016) 132–137.
- J. Di, J. Xia, M. Ji, B. Wang, S. Yin, Q. Zhang, Z. Chen, H. Li, Advanced photocatalytic performance of graphene-like BN modified BiOBr flower-like materials for the removal of pollutants and mechanism insight, *Appl. Catal. B Environ.* 183 (2016) 254–262.
- D.J. Fermin, E.A. Ponomarev, L.M. Peter, A kinetic study of CdS photocorrosion by intensity modulated photocurrent and photoelectrochemical impedance spectroscopy, *J. Electroanal. Chem.* 473 (1999) 192–203.
- V. Celorrio, L. Calvillo, E. Dann, G. Granozzi, A. Aguadero, D. Kramer, A.E. Russell, D.J. Fermin, Oxygen reduction reaction at La₂Ca_{1-x}MnO₃ nanostructures: interplay between A-site segregation and B-site valency, *Catal. Sci. Technol.* 6 (2016) 7231–7238.
- D.C. Green, S. Glatzel, A.M. Collins, A.J. Patil, S.R. Hall, A. New General, Synthetic strategy for phase-pure complex functional materials, *Adv. Mater.* 24 (2012) 5767–5772.
- V. Celorrio, E. Dann, L. Calvillo, D.J. Morgan, S.R. Hall, D.J. Fermin, Oxygen reduction at carbon-supported lanthanides: the role of the B-site, *ChemElectroChem* 3 (2016) 283–291.
- V. Celorrio, K. Bradley, O.J. Weber, S.R. Hall, D.J. Fermin, Photoelectrochemical properties of LaFeO₃ nanoparticles, *ChemElectroChem* 1 (2014) 1667–1671.
- V. Celorrio, D. Tiwari, D.J. Fermin, Composition-dependent reactivity of

- $Ba_{0.5}Sr_{0.5}Co_xFe_{1-x}O_{3-\delta}$ toward the oxygen reduction reaction, *J. Phys. Chem. C* 120 (2016) 22291–22297.
- [46] J. Tauc, R. Grigorovici, A. Vancu, Optical properties and electronic structure of amorphous germanium, *Phys. Status Solidi B* 15 (1966) 627–637.
- [47] B. Hou, D. Parker, G.P. Kissling, J.A. Jones, D. Cherns, D.J. Fermín, Structure and band edge energy of highly luminescent $CdSe_{1-x}Te_x$ alloyed quantum dots, *J. Phys. Chem. C* 117 (2013) 6814–6820.
- [48] M. Pourbaix, *Atlas of Electrochemical Equilibria in Aqueous Solutions*, Pergamon Press, Oxford, New York, 1966.
- [49] D.S. Bhachu, S.J.A. Moniz, S. Sathasivam, D.O. Scanlon, A. Walsh, S.M. Bawaked, M. Mokhtar, A.Y. Obaid, I.P. Parkin, J. Tang, C.J. Carmalt, Bismuth oxyhalides: synthesis, structure and photoelectrochemical activity, *Chem. Sci.* 7 (2016) 4832–4841.
- [50] W. Fan, C. Li, H. Bai, Y. Zhao, B. Luo, Y. Li, Y. Ge, W. Shi, H. Li, An in situ photoelectroreduction approach to fabricate Bi/BiOCl heterostructure photocathodes: understanding the role of Bi metal for solar water splitting, *J. Mater. Chem. A* 5 (2017) 4894–4903.
- [51] X. Liu, Y. Su, Q. Zhao, C. Du, Z. Liu, Constructing $Bi_{24}O_{31}Cl_{10}$ /BiOCl Heterojunction via a Simple Thermal Annealing Route for Achieving Enhanced Photocatalytic Activity and Selectivity, *Vol. 6* (2016), p. 28689.
- [52] A. Gomis-Berenguer, V. Celorrio, J. Iniesta, D.J. Fermin, C.O. Ania, Nanoporous carbon/ WO_3 anodes for an enhanced water photooxidation, *Carbon* 108 (2016) 471–479.
- [53] X. Tu, S. Luo, G. Chen, J. Li, One-pot synthesis, characterization, and enhanced photocatalytic activity of a BiOBr–graphene composite, *Chem. Eur. J.* 18 (2012) 14359–14366.